# A Monte Carlo simulation study of the ionic liquid 1-n-butyl-3-methylimidazolium hexafluorophosphate: Liquid structure, volumetric properties and infinite dilution solution thermodynamics of $CO_2$

Jindal K. Shah and Edward J. Maginn
*Department of Chemical and Biomolecular Engineering,*
*University of Notre Dame, Notre Dame, IN 46556, USA*

**Abstract**

A Monte Carlo simulation study is performed on the ionic liquid 1-n-butyl-3-methylimidazolium hexafluorophosphate. A modified united atom forcefield is developed for the ionic liquid. Volumetric properties such as density, isothermal compressibility and volume expansivity are computed at temperatures ranging from 298 K to 343 K. Henry's constants and infinite dilution enthalpies and entropies of absorption are computed for $CO_2$ in the ionic liquid. In addition, local structural information is obtained from radial distribution function analysis. Comparison is made between calculated properties and available experimental data. The performance of the new forcefield is assessed by comparison with two other forcefields developed for this compound.

## Introduction and Motivation

Ionic liquids are salts that remain liquid down to temperatures near or below ambient. These compounds have become the subject of intense study in recent years [1] as researchers have sought to understand and exploit their unusual properties. Ionic liquids have excellent solvation properties and are completely non-volatile, thus making them potentially useful as environmentally benign solvents. In fact, the first commercial process to utilize ionic liquids was recently announced [2] and several other companies have started active research programs in this area.

The most widely studied class of ionic liquids to date is based on a dialkylimidazolium cation with an inorganic anion such as hexafluorophosphate or tetrafluoroborate. It is possible to make ionic liquids with a wide range of other cation classes, however, such as alkylpyridinium, dialkylpyrrolidinium and quaternary ammonium. A host of other anions can also be used, such as nitrate, acetate, trifluoroacetate and bis(trifluoromethylsulfonyl) imide, to name just a few. As has been pointed out [3], the number and diversity of these species and their mixtures means that it is possible to envision something on the order of $10^9$ different ionic liquids. Determining which of these liquids has the right properties for a given application is a daunting task. For this reason, recent efforts have been directed at using molecular modeling to relate chemical structure and constitution to important thermophysical properties.

The earliest theoretical calculations performed on compounds that fit the contemporary definition of an ionic liquid involved the use of semi-empirical molecular orbital calculations to determine optimized geometries and cation reduction potentials [4], [5]. Higher level quantum calculations have subsequently been used to examine structures of gas phase ion pairs [6]. Classical simulations have also been used to compute condensed phase properties. Hanke et al. [7] developed explicit hydrogen (all atom) and united atom forcefields for the dimethylimidazolium cation paired with chloride and hexafluorophosphate anions. They computed structural, volumetric and dynamic properties of the pure liquids for temperatures ranging from 400-500 K. This group also investigated the solvation of small molecules in dimethylimidazolium chloride at 400 K using molecular dynamics and thermodynamic integration [8], [9]. Although direct comparison with experiment was not possible due to a lack of data, these authors point out that their values are consistent with experimental results [10] for water solubility in 1-n-butyl-3-methylimidazolium hexafluorophosphate [bmim][$PF_6$]. Owing to the fact that the most commonly studied ionic liquid to date from an experimental standpoint is [bmim][$PF_6$], Shah et al. [11] developed a united atom (no explicit hydrogens or fluorines) forcefield for this compound. They computed various volumetric properties using Monte Carlo, and found reasonably good agreement with experiment. More detailed forcefields containing explicit hydrogens and fluorines were subsequently developed for the same compound independently by Margulis et al. [12] and Morrow and Maginn [13]. Margulis and co-workers simulated the pure liquid at 303 K and 0.98 bar, computing the density, radial distribution function, local dynamics and the self-diffusivity. The calculated density was within about 5 % of the experimental value. Morrow and Maginn performed simulations at 0.98 bar and at temperatures ranging from 298-343 K. Densities were within 1 % of the experimental values, while derivative quantities such as volume expansivities and isothermal compressibilities deviated anywhere from 10-40 % from experiment. Self-diffusivites and local dynamics were similar to those computed using the forcefield from reference [12]. A forcefield for the [bmim] and 1-ethyl-3-methylimidazolium (emim) cations paired with tetrachloraluminate and tetrafluoroborate anions was developed and tested by de Andrade et al. [14], [15]. Pure component densities were found to deviate from experiment by less than 1 %. Local structure, in the form of a

radial distribution function, was found to agree very well with experimental neutron diffraction data [15].

These results demonstrate that classical molecular mechanics-based methods can be used to accurately compute some properties of ionic liquids. However, much work remains to be done, and a great number of questions remain unanswered. First, all but two [8], [9] of the previous condensed phase studies focused only on pure liquid properties. Understanding the properties of mixtures containing ionic liquids is essential for the development and utilization of these compounds, and molecular simulations are an ideal tool for obtaining this understanding. Second, due in large part to a lack of experimental data, direct comparison with experiment has been limited mainly to densities. However, it is well known that liquid density is not a particularly sensitive measure of the accuracy or suitability of a forcefield. This is one reason why forcefields with quite different parameters can yield similar liquid densities. Derivative quantities such as the volume expansivity and isothermal compressibility, as well as vapor-liquid equilibria data, are much more stringent tests of a forcefield than density [16]. Third, most calculations have been done at a single temperature and pressure, or over a narrow range of temperature. Most of the applications envisioned for ionic liquids will occur at a range of temperatures and pressures, and so forcefields need to be tested at a variety of statepoints. Finally, the all atom forcefields were found to yield somewhat more accurate densities than the simpler united atom forcefield for [bmim][$PF_6$] [11]-[15]. However, the computational cost of an all atom forcefield is considerably higher than that for a united atom forcefield. It would be desirable to determine how detailed a forcefield must be to obtain a given level of accuracy, and to understand how the different elements of a forcefield affect the accuracy of the results.

The present study is a first step in addressing the above issues. An extension is made to our previous united atom model [11] for [bmim][$PF_6$]. The accuracy of the forcefield in predicting density, isothermal compressibility and volume expansivity at three temperatures is tested by direct comparison with experimental data [17] as well as simulation results obtained with other forcefields. In addition, Henry's constants as well as enthalpies and entropies of absorption for $CO_2$ at infinite dilution are computed and compared against experimental data [18].

## Simulation Details

### Forcefield

A standard fuctional form [19] was used to describe the total energy of the system $\mathcal{V}_{tot}$

$$\mathcal{V}_{tot} = \sum_{ij}\left[4\epsilon_{ij}\left(\left(\frac{\sigma_{ij}}{r_{ij}}\right)^{12} - \left(\frac{\sigma_{ij}}{r_{ij}}\right)^{6}\right) + \frac{q_i q_j}{r_{ij}}\right] + \mathcal{V}(\phi) \quad (1)$$

TABLE I: Cartesian coordinates of the optimized geometry of the united atom representation of [bmim][$PF_6$] in Angstrom.

| Atom | X | Y | Z | Atom | X | Y | Z |
|---|---|---|---|---|---|---|---|
| $N_1$ | -2.0478 | 0.682 | 0.272 | $C_2$ | -1.322 | -0.100 | -0.530 |
| $N_3$ | -2.041 | -1.177 | -0.852 | $C_4$ | -3.274 | -1.083 | -0.232 |
| $C_5$ | -3.279 | 0.082 | 0.469 | $C_6$ | -1.542 | -2.310 | -1.640 |
| $C_7$ | -1.574 | 1.940 | 0.888 | $C_8$ | -1.993 | 3.187 | 0.103 |
| $C_9$ | -1.340 | 3.348 | -1.278 | $C_{10}$ | 0.173 | 3.582 | -1.238 |
| $P$ | 1.995 | -1.001 | 0.512 | $F_1$ | 1.428 | -1.098 | -1.066 |
| $F_2$ | 0.502 | -1.550 | 1.005 | $F_3$ | 2.527 | -2.527 | 0.414 |
| $F_4$ | 2.462 | -0.861 | 2.055 | $F_5$ | 3.400 | -0.413 | -0.031 |
| $F_6$ | 1.366 | 0.553 | 0.557 | | | | |

The sum is carried out over all interaction sites i and j on different molecules, and between sites on the same molecule separated by more than three bonds. The energy arising due to the internal rotations of the four dihedral angles associated with the butyl group on the cation is included in the valence term $\mathcal{V}(\phi)$, which is given by the following Fourier series

$$\mathcal{V}(\phi) = \mathcal{V}_0 + \frac{\mathcal{V}_1}{2}(1+\cos(\phi)) + \frac{\mathcal{V}_2}{2}(1-\cos(2\phi)) + \frac{\mathcal{V}_3}{2}(1+\cos(3\phi)) \quad (2)$$

where $\phi$ is the torsion angle and $\mathcal{V}_1, \mathcal{V}_2, \mathcal{V}_3$ are the Fourier coefficients. The parameters for eqs. 1 and 2 were determined in the following manner.

First, *ab initio* calculations were carried out on an isolated cation-anion pair in the gas phase using *Gaussian* 98© [20] at the B3LYP/6-311+G* level. The resulting minimum energy structure for the cation and anion was used to set bond lengths, bond angles and the imidazolium ring geometry. These intramolecular coordinates, shown in Table I, were held fixed in all the simulations. Partial charges on each atom were determined by fitting to the electrostatic potential at points selected according to the CHELPG method [21]. This resulted in a net charge of 0.904 and -0.904 on the cation and anion respectively. The united atom representation of the cation utilized in our previous study [11] was adopted. That is, all hydrogen atoms were subsumed into the carbon atom centers to which they were bonded. The $[PF_6]^-$ was described using a seven-site model with the phosphorus and fluorine interaction sites located at the respective atomic centers as shown in Fig. 1. The Lennard-Jones parameters for $[PF_6]^-$ were obtained from reference [22] while for the cation they were taken from [11]. Cross interactions involving unlike atom types were set by using a standard Lorentz-Bethelot combining rule [19]. The Lennard-Jones interaction parameters and partial charges of all the atoms are given in Table II. A listing of all the dihedral angles considered for internal rotation and the Fourier coefficient associated with each rotation are provided in Table III. We will refer to this revised united atom forcefield as UA2, while the original united atom forcefield of reference [11] will be referred to as UA1 and

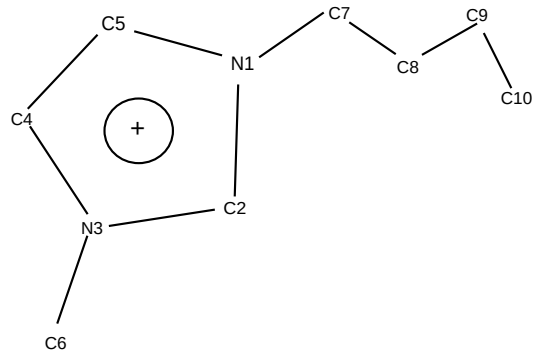


FIG. 1: Atom numbering scheme used in the current work

TABLE II: Forcefield parameters used in this work.

| Atom | $\sigma_{ii}$ /Å | $\epsilon$ /$kJ\,mol^{-1}$ | $q_i/e$ |
|---|---|---|---|
| $N_1$ | 3.250 | 0.710 | 0.111 |
| $N_3$ | 3.250 | 0.710 | 0.133 |
| $C_2$ | 3.880 | 0.443 | 0.233 |
| $C_4$ | 3.880 | 0.443 | 0.040 |
| $C_5$ | 3.880 | 0.443 | -0.010 |
| $C_6$ | 3.775 | 0.865 | 0.183 |
| $C_7$ | 3.905 | 0.493 | 0.195 |
| $C_8$ | 3.905 | 0.493 | -0.066 |
| $C_9$ | 3.905 | 0.493 | 0.128 |
| $C_{10}$ | 3.905 | 0.732 | -0.043 |
| $P$ | 3.740 | 0.836 | 1.460 |
| $F$ | 3.118 | 0.255 | -0.394 |

the all atom forcefield of reference [13] will be referred to as AA. One of the objectives of this study is to determine the predictive capability of UA2 relative to the two other forcefields. Note that in none of the cases have forcefield parameters been adjusted to match experimental data.

### NPT simulations

Monte Carlo simulations were performed in the isothermal-isobaric (NPT) ensemble using Metropolis acceptance rules. The system consisted of a total of 250 cations and 250 anions in a cubic simulation box with standard periodic boundary conditions. Electrostatic interactions were computed using the Ewald summation method [19] with the permittivity of the surrounding medium set to unity. A spherical cutoff equal to half the box length was used for Lennard-Jones interactions. Standard long range corrections were applied beyond the cutoff distance. A hard sphere cutoff was employed to immediately reject any move bringing two atoms closer than 1 Å.

Initial configurations were generated by randomly inserting 25 cation and anion pairs into the simulation box, after which the system was relaxed by performing standard displacement and rotational moves for a few cycles. A cycle refers to the set of moves in which each molecule in the simulation box is moved at least once. The procedure was repeated until all the ions were added to the system. Two sets of initial configurations were obtained in this manner, one at the experimental density and the other at a lower density. These configurations were subsequently equilibrated in a two step procedure. For the first 2000 cycles, the simulation was carried out in the canonical ensemble using three types of moves: translation of an ion center-of-mass (COM); rotation about a randomly chosen axis through the COM; and rearrangement of one of the torsion angles in the butyl chain. The boldness of these moves was adjusted to yield roughly 50% acceptance, and was then unchanged for the remainder of the simulation. In the second phase of equilibration, 50000 to 60000 cycles were run in the isothermal-isobaric ensemble. In addition to the three moves described above, one volume perturbation was performed each cycle. Upon observation of steady state density and energy, the system was assumed to be equilibrated. Ensemble averages were then accumulated during the production phase over 10000 to 15000 cycles. Four independent simulations at a given statepoint were conducted. Reported values were obtained by averaging the results of these four simulations. Error bars were estimated from the standard deviation.

TABLE III: Torsional parameters for the rotatable dihedral angles.

| Dihedral Angle | $V_0$ | $V_1$ | $V_2$ | $V_3$ |
|---|---|---|---|---|
| | | $kJ\,mol^{-1}$ | | |
| $C_7-C_8-C_9-C_{10}$ | 0.00 | 5.89 | -1.13 | 13.17[a] |
| $N_1-C_7-C_8-C_9$ | 0.00 | 11.41 | 0.96 | 2.05[b] |
| $C_2-N_1-C_7-C_8$ | 0.00 | -5.85 | -1.80 | 0.00[c] |
| $C_5-N_1-C_7-C_8$ | 0.00 | -5.85 | -1.80 | 0.00[c] |

a. OPLS-UA parameters for *n*-alkane
b. OPLS-AA parameters for *n*-ethylformamide
c. OPLS-AA parameters for ammonium ion

### Results and Discussion

The density, volume expansivity, isothermal compressibility, local fluid structure and Henry's constant for $CO_2$ were computed at three temperatures, 298 K, 323 K and 343 K. Results were compared both with experimental data [17] and simulation results obtained using the UA1 and AA forcefields.

### Liquid Density

The density of the pure IL was obtained as an ensemble average during the production phase of the NPT simulation. In Fig. 2, predictions of density as a function of

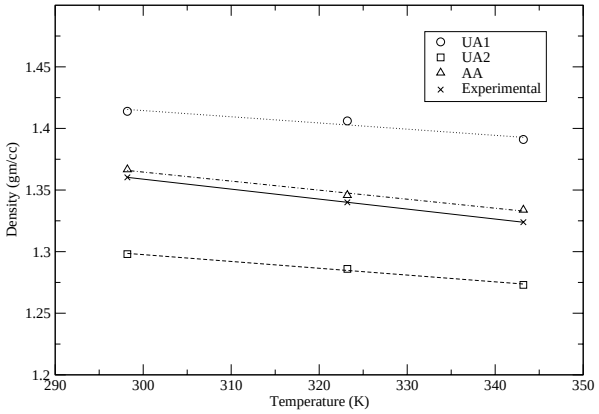


FIG. 2: Comparision of the density as a function of temperature predicted by the different forcefields with experimental results of Gu and Brennecke [17].

temperature obtained using the different forcefields are compared against experimental data. The lines are linear fits to the data. Numerical results are provided in Table IV. At each temperature, UA2 predicts densities that are lower than the experimental values by approximately $3-5\%$. This level of agreement is similar to that observed with UA1 and the all atom forcefield of reference [12], and indicates reasonable accuracy, considering that no adjustments were made to the parameters to reproduce the experimental densities. It is interesting to note that while the magnitude of the discrepancy for UA1 and UA2 is roughly the same, UA1 *over predicts* the density, while UA2 *under predicts* the density. There are two major differences between UA1 and UA2 that are responsible for this difference. First, the net charge of the ions is different in the two models. In UA1, the ions are assumed to have a net charge of $\pm$ 1, while in UA2 the net charge is lowered to $\pm$ 0.904. This reduction in net charge arises from the fact that in the gas phase quantum calculations used to determine the partial charges for UA2, some charge transfer is observed to take place between the two ions, thereby lowering the net charge of each ion. The reduction in net charge can be expected to result in a weakening of the electrostatic attraction between the cation and anion, and thus a reduction in the liquid density. Second, the $[PF_6]^-$ is represented in atomistic detail in UA2, but is treated as a sphere with -1 charge in UA1. Apparently, the spherical anion of UA1 can pack more efficiently than can the "atomically rough" anion of UA2, thereby increasing the density. In both cases, one expects the distance between cations and anions to be greater for UA2 than for UA1, which is indeed observed in radial distribution functions (see below). Finally, we note that the AA model is best able to reproduce experimental densities, showing less than 1 % deviation from

TABLE IV: Comparison of density predictions by different forcefields with experimental results from 298 K to 343 K at atmospheric pressure. Experimental data from [17], UA1 results are from [11] and AA results are from [13]. The numbers in parenthesis indicate the uncertainty in the last decimal place.

| Temperature /$K$ | UA1 | UA2 | AA | Exp. |
|---|---|---|---|---|
| | | gm/cm$^3$ | | |
| 298 | 1.414(3) | 1.298(3) | 1.3667 | 1.3603(8) |
| 323 | 1.406(2) | 1.286(3) | 1.3458 | 1.340(8) |
| 343 | 1.391(2) | 1.273(3) | 1.339 | 1.324(8) |

experimental densities. This level of accuracy could be fortuitous, or it may indicate that the added realism of the hydrogen atoms on the imidazolium ring and alkyl groups is necessary to capture subtle packing effects for this liquid.

### Volume Expansivity

The change in density of a substance with temperature is generally quantified by the volume expansivity, defined as

$$\alpha_P = -\frac{1}{\rho}\left(\frac{\partial \rho}{\partial T}\right)_P \tag{3}$$

where $\rho$ is the liquid density. The volume expansivity can be estimated from eqn. 3 by conducting a series of simulations at constant pressure but at different temperatures. Since the density typically varies linearly with temperature over small temperature ranges, $\alpha_p$ can be determined from a linear fit of density versus temperature data, as shown in Fig. 2. Results computed using the different forcefields are compared against one another and experiment in Table V. The computed $\alpha_P$ is relatively constant over the temperature range, a trend also observed experimentally. It can be concluded from Table V that the UA2 forcefield is somewhat better than the UA1 forcefield in predicting volume expansivity. This improvement may be due to the decreased electrostatic interaction between the ions in UA2 relative to UA1. The AA forcefield yields results that are even closer to experimental values than those obtained using UA2.

### Isothermal Compressibility

The change in molar volume of a substance with pressure at a given temperature is described by the isothermal compressibility, defined as

$$\kappa_T = -\frac{1}{V}\left(\frac{\partial V}{\partial P}\right)_T \tag{4}$$

TABLE V: Comparison of volume expansivity predictions by differenet forcefields with experimental results from 298 K to 343 K.

| Temperature / K | $\alpha^1_{exp}$ | $\alpha^2_{sim}$ | $\alpha^3_{sim}$ | $\alpha^4_{sim}$ |
|---|---|---|---|---|
| | x $10^4$ $K^{-1}$ | | | |
| 298 | 6.11 | 3.52 | 4.34 | 5.49 |
| 323 | 6.02 | 3.50 | 4.30 | 5.42 |
| 343 | 5.94 | 3.46 | 4.25 | 5.36 |

1. Experimentally determined [17].
2. United atom forcefield UA1 [11].
3. United atom forcefield UA2.
4. All atom forcefield AA [13].

TABLE VI: Comparsion of experimentally determined isothermal compressibility with the predictions by different forcefields for temperatures ranging from 298 K to 343 K

| Temperature / K | $\kappa^1_{exp}$ | $\kappa^2_{sim}$ | $\kappa^3_{sim}$ | $\kappa^4_{sim}$ |
|---|---|---|---|---|
| | x $10^{11}$ $Pa^{-1}$ | | | |
| 298 | 41.95 | $N/A$ | 49.04 | 36.83 |
| 323 | 49.35 | 29.6 | 31.21 | 32.86 |
| 343 | $N/A$ | $N/A$ | 32.11 | 39.20 |

1. Experimentally determined [17].
2. Fluctuation formula eqn. 5, UA1 [11]
3. Fluctuation formula eqn. 5, UA2
4. Fluctuation formula eqn. 5, AA [13]

In an isothermal-isobaric ensemble simulation, fluctuations in the system volume are monitored and $\kappa_T$ is computed as [19]

$$\kappa_T = \frac{\langle V^2 \rangle - \langle V \rangle^2}{k_B T \langle V \rangle} \tag{5}$$

where $\langle\rangle$ denotes an NPT ensemble average. The computed values of $\kappa_T$ for different forcefields are summarized in Table VI. Experimental $\kappa_T$ values are also listed. Overall the UA2 model predicts $\kappa_T$ values that are in reasonable agreement with experiment. It appears to be somewhat better than the UA1 model, and nearly equivalent to the AA model for this property. Results deviate from the experimental values by $16-36\%$, which is reasonably good, considering the well known difficulties associated with computing derivative quantities such as $\kappa_T$ using fluctuation methods.

### Radial Distribution Functions

The relatively good agreement between experimental temperature-volume properties and those obtained using the UA2 forcefield provides confidence that the actual fluid structure should be in good accord with that determined from simulations. To gain a better understanding of the organization of ions in the liquid, various radial distribution functions (RDFs) were computed. In particular, the center-of-mass (COM) RDFs between cation-cation, cation-anion and anion-anion were calculated and differences between those obtained from the other forcefields were examined. As the RDFs are very similar at each of the three temperatures examined, we focus only on the results at 298 K. One of the most interesting RDFs that provides insight into local fluid structure is that between cation and anion centers of mass.

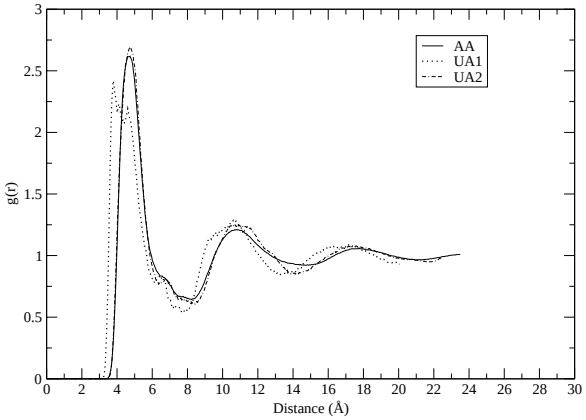


FIG. 3: Center of mass radial distribution functions for the cation and anion obtained from the three forcefields at 298 K.

Fig 3 shows the COM cation-anion RDF for all the forcefields at 298K. The RDFs are qualitatively similar to each other, but differences can be seen, particularly in the first solvation shell. The peak height and location of the first solvation shell is nearly identical for UA2 and AA, but UA1 shows a split peak nearly 1 Å closer than for the other two RDFs. Thus, the UA1 forcefield enables a closer approach between centers of mass of cations and anions. As mentioned earlier, this is likely due to the fact that the anion is spherical in UA1, and that each ion has a slightly larger net charge when compared to the other two forcefields. These two effects enable the ions to approach closer than with the other forcefields.

In addition to the COM radial distribution functions, additional information on local fluid structure can be extracted by examining specific site-site RDFs. In particular, it is instructive to investigate the RDFs for the phosphorus atom of the anion and different imidazolium ring carbon atoms. Figure 4 shows the RDF between the P atom on the anion and the C2 carbon on the imidazolium ring.

All three forcefields show a strong localization of the anion about the C2 position, as demonstrated by the large, sharp first peak in the RDF at about 4 Å. The first peak is at a slightly greater distance for UA2 than for the other models, but the differences are quite small.

For the association of the anion with the other ring

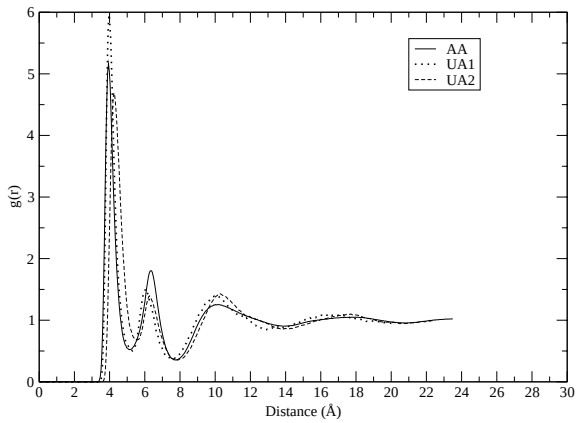


FIG. 4: Radial distribution functions for the anion P atom and the C2 carbon on the imidazolium ring at 298 K.

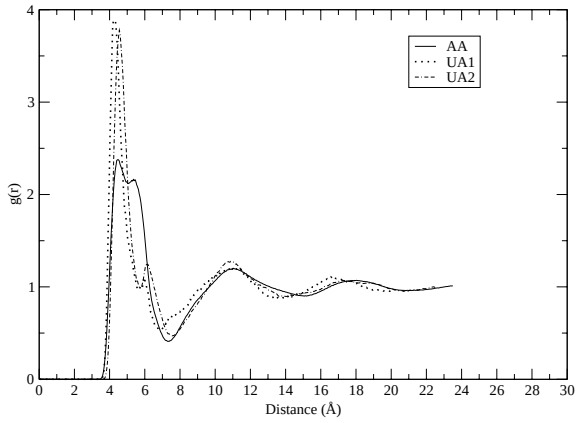


FIG. 5: Radial distribution functions for the anion P atom and the C4 carbon on the imidazolium ring at 298 K.

carbons (C4 and C5), the differences between the RDFs obtained from the three forcefields are greater. Figure 5 shows the P-C4 RDF, while figure 6 shows the P-C5 RDF.

The AA forcefield shows a broader, more diffuse first peak for both carbon atoms, whereas the two united atom forcefields show sharper peaks. This indicates that the presence of the hydrogen atom bonded to the C4 and C5 carbons in the AA forcefield screens the association of the anion with the ring carbon atoms, decreasing the ordering of the anion about this side of the ring. On the other hand, the united atom forcefields allow more localized, direct organization of the anion about the ring carbon atoms. Longer range order (beyond 1 nm) is similar for all forcefields.

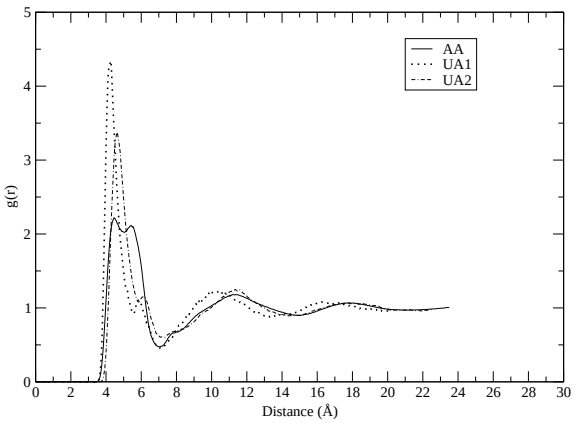


FIG. 6: Radial distribution functions for the anion P atom and the C5 carbon on the imidazolium ring at 298 K.

### Henry's Constant of $CO_2$

The solubility of a dilute solute 2 in a solvent 1 is generally expressed in terms of Henry's law, which relates the fugacity of species 2 in the liquid state to its mole fraction $x_2$ via the following relation

$$f_2 = H_{2,1} x_2 \tag{6}$$

where $H_{2,1}$ denotes the Henry's constant of solute 2 in the solvent 1. Formally, the Henry's constant is defined as

$$H_{2,1} = \lim_{x_2 \to 0} \frac{f_2}{x_2} \tag{7}$$

In a simulation, the Henry's constant can be calculated from the following expression

$$H_{2,1} = k_B T \rho_1 exp(\beta \mu_2^{ex}) \tag{8}$$

where $\rho_1$ is the liquid density and $\beta = 1/k_B T$. The excess chemical potential ($\mu_2^{ex}$) of solute ($CO_2$) may be computed in a variety of ways. In the present work, $\mu_2^{ex}$ was computed using the test-particle insertion method [24]. During the course of the NPT simulations, 900 uncorrelated configurations were saved to disk. For each of these configurations, 100000 $CO_2$ "test" molecules were inserted at random positions and orientations, and the excess chemical potential was determined from the following relation [25]

$$\mu_2^{ex} = -k_B T \ln \frac{\langle V exp(-\beta U_g) \rangle}{\langle V \rangle} \tag{9}$$

where $U_g$ is the interaction of the $CO_2$ molecules with all the ionic liquid molecules. The test particle method is known to be subject to systematic errors, especially

TABLE VII: Comparison between results of $CO_2$ Henry's constant from simulations and experiments

| Temperature / K | $H^1_{exp}$ | $H_{sim}$ |
|---|---|---|
| | bar | |
| 298.2 | $53.4 \pm 0.3$ | $18.0 \pm 2.0$ |
| 323.2 | $81.3 \pm 0.5$ | $49.3 \pm 10.0$ |
| 343.2 | $150.0 \pm 1.0^2$ | $60.0 \pm 15.0$ |

1. Experiments [18].
2. Estimated from experimental data using eqn. 11.

for systems like the one under study that consists of a dense liquid phase with strong interactions. More sophisticated sampling procedures could be applied to obtain a more reliable estimate of the Henry's constant, and this is planned for future work. Nevertheless, the test particle method is expected to give reasonably good estimates of the Henry's constant for this system, especially given the extensive sampling employed.

The values for the Henry's constant of $CO_2$ in [bmim][$PF_6$] calculated from simulations with the UA2 forcefield are listed in Table VII. Error bars were determined from the fluctuations in the running average of the Henry's constant. The simulations predict Henry's constants that are consistently lower than experimental values by a factor of $2-2.5$, indicating greater solubility than what is observed experimentally [18]. This level of agreement between experimental and simulated Henry's constant is typical of results obtained with other systems, including n-butane and n-hexane in water [26] and cyclohexane in water [27]. Given the fact that previous experimental studies show that Henry's constants in this ionic liquid vary over five orders of magnitude in going from a highly soluble compounds like water to relatively insoluble species like argon [10],[18], the level of agreement between experiment and simulation is encouraging.

### Enthalpy and Entropy of absorption

By considering the dependence of the Henry's constant on temperature, the enthalpy and entropy of absorption can be calculated as [10]

$$\Delta h_2 = \overline{h}_2 - h_2^{ig} = R\left(\frac{\partial \ln H_{2,1}}{\partial\left(\frac{1}{T}\right)}\right)_P \tag{10}$$

$$\Delta s_2 = \overline{s}_2 - s_2^{ig} = R\left(\frac{\partial \ln H_{2,1}}{\partial \, lnT}\right)_P \tag{11}$$

where $\overline{h}_2$ and $\overline{s}_2$ are the partial molar enthalpy and entropy of a pure solute in the solution, while $h_2^{ig}$ and $s_2^{ig}$ are the ideal gas phase values of enthalpy and entropy of the solute at the given state point (T,P). The enthalpy provides information about the strength of interaction between the IL and solute, while the entropy provides an indication the level of ordering that takes place in the IL/solute mixture [18].

TABLE VIII: Experimental and simulation values for heat of absorption and entropy of absorption of $CO_2$ in [bmim][$PF_6$]

| | $\Delta h_2$ $kJ\,mol^{-1}K^{-1}$ | $\Delta s_2$ $J\,mol^{-1}K^{-1}$ |
|---|---|---|
| Simulation | $-16.51$ | $-72.95$ |
| Experiment | $-16.1 \pm 2.2$ | $-53.2 \pm 6.9$ |

The enthalpy and entropy values for dissolution of $CO_2$ are listed in Table VIII along with those experimentally obtained [18]. The agreement between the simulated and experimental enthalpy is remarkably good. This implies that the energetic interactions between $CO_2$ and the ionic liquid are captured well by the model. The entropy of absorption is also captured well by the simulations, althouogh the percent deviation is greater than for the enthalpy. It is important to note, however, that the magnitude of $\Delta s_2$ is much smaller than $\Delta h_2$, and so it is more difficult to obtain with a high precision.

### Conclusions

Monte Carlo simulations have been conducted to compute properties for 1-n-butyl-3-methylimidazolium hexafluorophosphate, a widely studied ionic liquid. A modified united atom forcefield was developed and employed, and its performance assessed by comparing computed properties against experimental data. Specifically, volumetric properties such as density, isothermal compressibility and volume expansivity were computed and found to be in reasonable agreement with recent experimental data. Henry's constants as well as the enthalpy and entropy of absorption for $CO_2$ were also computed and compared against experiment. Computed Henry's constants predict slightly greater solubility of $CO_2$ than what is observed experimentally, although a near quantitative agreement is obtained between the computed and experimental enthalpy and entropy of absorption. The performance of this forcefield in predicting volumetric properties relative to a more detailed all atom model and a coarser-grained model was also discussed.

### Acknowledgement

Funding for this research was provided by the National Science Foundation (CT99-97626).

[1] J. F. Brennecke and E. J. Maginn, AIChE J, 47 (2001) 2384-2389.
[2] M. Freemantle, Chemical and Engineering News, 81, (2003) 9.
[3] J. D. Holbrey and K. R. Seddon, Clean Products and Processes, 1 (1999) 223-236.
[4] J. S. Wilkes, Green Chemistry, 4, (2002) 73-80.
[5] C. J. Dymek Jr., and J. J. P. Stewart, Inorganic Chem., 28 (1989) 1472-1476.
[6] Z. Meng, A. Dölle, and W. R. Carper, J. Molec. Struct. (Theochem), 585 (2002) 119-128.
[7] C. G. Hanke, S. L. Price and R. M. Lynden-Bell, Mol.Phys. 99 (2001) 801-809.
[8] C. G. Hanke, N. A. Atamas, and R. M. Lynden-Bell, Green Chem., 4 (2002) 107-111.
[9] R. M. Lynden-Bell, N. A. Atamas, A. Vasilyuk and C. G. Hanke, Molec. Phys., 100 (2002) 3225-3229.
[10] J. L. Anthony, E. J. Maginn and J. F. Brennecke, J. Phys. Chem. B, 105 (2001) 10942-10949.
[11] J. K. Shah, J. F. Brennecke and E. J. Maginn, Green. Chem., 4 (2002) 112-118.
[12] C. J. Margulis, H. A. Stern and B. J. Berne, J. Phys. Chem. B, 106 (2002) 12017-12021.
[13] T. I. Morrow and E. J. Maginn, J. Phys. Chem. B., 106 (2002) 12807-12813
[14] J. de Andrade, E. S. Böes and H. Stassen, J. Phys. Chem. B, 106 (2002) 3546-3548.
[15] J. de Andrade, E. S. Böes and H. Stassen, J. Phys. Chem. B, 106 (2002) 13344-13351.
[16] G. C. Boulougouris, I. G. Economou and D. N. Theodorou, J. Phys. Chem. B, 102 (1998) 1029-1035.
[17] Z. Y. Gu, J. F. Brennecke, J. Chem. Eng. Data, 47 (2002) 339-345.
[18] J. L. Anthony, E. J. Maginn and J. F. Brennecke, J. Phys. Chem. B, 106 (2002) 7315-7320.
[19] M. P. Allen and D. J. Tildesley, Computer Simulation of Liquids, Oxford University Press, New York, 1990.
[20] M. J. Frisch, G. W. Trucks, et al., Gaussian 98, revision A.9, Gaussian Inc., Pittsburgh, PA, 1998.
[21] C. M. Breneman and K. B. Wiberg, J. Comput. Chem., 11 (1990) 361-373.
[22] G. A. Kaminksi and W. L. Jorgensen, J. Chem. Soc. Perkin. Trans., 2 (1999) 2365-2375.
[23] J. J. Potoff and J. I. Siepmann, AIChE J., 47 (2001), 1676-1682.
[24] B. Widom, J. Chem. Phys., 39 (1963) 2808-2812.
[25] K. S. Shing and S. T. Chung, J. Phys. Chem., 91 (1987) 1674-1681.
[26] G. C. Boulougouris, J. R. Errington, I. G. Economou, A. Z. Panagiotopoulos and D. N. Theodorou, J. Phys. Chem. B, 2000 (104) 4958-4963.
[27] J. R. Errington and A. Z. Panagiotopoulos, J. Chem. Phys., 111 (1999) 9731-9738.